Functions of His107 in the Catalytic Mechanism of Human Glutathione *S*-Transferase hGSTM1a-1a[†,‡]

Yury V. Patskovsky, Larysa N. Patskovska, and Irving Listowsky*

Department of Biochemistry, Albert Einstein College of Medicine, Bronx, New York 10461

Received September 10, 1998; Revised Manuscript Received November 30, 1998

ABSTRACT: Domain interchange analyses and site-directed mutagenesis indicate that the His107 residue of the human subunit hGSTM1 has a pronounced influence on catalysis of nucleophilic aromatic substitution reactions, and a H107S substitution accounts for the marked differences in the properties of the homologous hGSTM1-1 (His107) and hGSTM4-4 (Ser107) glutathione *S*-transferases. Reciprocal replacement of His107 and Ser107 in chimeric enzymes results in reciprocal conversion of catalytic properties. With 1-chloro-2,4-dinitrobenzene as a substrate, the His107 residue primarily influences the pH dependence of catalysis by lowering the apparent pK_a of k_{cat}/K_m from 7.8 for the Ser107-containing enzymes to 6.3 for the His107-containing enzymes. There is a parallel shift in the pK_a for thiolate anion formation of enzyme-bound GSH. Y6F mutations have no effect on the pK_a for these enzymes. Crystal structures of hGSTM1a-1a indicate that the imidazole ring of His107 is oriented toward the substrate binding cleft approximately 6 Å from the GSH thiol group. Thus, His107 has the potential to act as a general base in proton transfer mediated through an active site water molecule or directly following a modest conformational change, to promote thiolate anion formation. All wild-type enzymes and H107S chimera have nearly identical equilibrium constants for formation of enzyme−GSH complexes (K_d values of $1-2 \times 10^{-6}$ M); however, K_m^{GSH} and K_i values for *S*-methylglutathione inhibition determined by steady-state kinetics are nearly 100-fold higher. The functions of His107 of hGSTM1a-1a are unexpected in view of a substantial body of previous evidence that excluded participation of histidine residues in the catalytic mechanisms of other glutathione *S*-transferases. Consequences of His107 involvement in catalysis are also substrate-dependent; in contrast to 1-chloro-2,4-dinitrobenzene, for the nucleophilic addition reaction of GSH to ethacrynic acid, the H107S substitution has no effect on catalysis presumably because product release is rate-limiting.

Glutathione *S*-transferases (GSTs)[1] catalyze nucleophilic substitution and addition reactions between GSH and a vast array of aromatic and aliphatic electrophilic compounds (*1*−*3*). Because alkylating agents, including antineoplastic drugs and certain cytotoxic, genotoxic, or carcinogenic agents, are substrates for these enzymes, GSTs are considered to function in detoxification or chemoprotective capacities (*4*−*8*). Mammalian GSTs are products of gene superfamilies (*9*−*11*), and cytosolic forms of the enzymes have been subdivided into Alpha, Mu, Pi, and Theta classes in a species-independent nomenclature system based on primary structure homologies, dimeric subunit assembly patterns, and certain other common properties (*11, 12*).

The human class Mu GSTs, particularly the hGSTM1, hGSTM2, hGSTM4, and hGSTM5 subunits,[2] whose amino acid sequences are more than 85% identical (and more than 80% with most rodent class Mu GSTs), represent a series of structural homologues with sufficient, albeit limited, structural divergence to result in different catalytic efficiencies and substrate specificities. These closely related proteins may thus be employed as convenient natural models to evaluate catalytic mechanisms of the GSTs. There are five human class Mu GST genes clustered on band 1p13.3 of chromosome 1 (*13*), and four of these (*hGSTM1*, *hGSTM2*, *hGSTM4*, and *hGSTM5*) probably originated from mechanisms involving gene conversions (*13*−*15*). The hGSTM1 GST has attracted considerable attention because a gene deletion occurs with high frequency so that about 50% of the human population are *hGSTM1*-null. The GSTM1-1 enzyme, which is a major GST in liver (*16*), has a relatively high conjugating activity with various aromatic epoxides, including some which are chemical carcinogens (*17*). Thus, extensive epidemiological studies were performed in an attempt to correlate the *hGSTM1*-null phenotype and cancer development (*18*). GSTs are thought to enhance the reactivity of bound GSH by lowering the pK_a of its sulfhydryl group with the thiolate anion acting as the reactive nucleophile (*19*, *20*). Chimeric GSTs have been used to probe structure−activity relationships of GSTs (*21*). Although it is reasonable to suppose that a histidine residue could be involved in the proton transfer from the thiol at physiological pH values, considerable experimental efforts have failed to verify that

[†] This work was supported by Grant CA42448 from the National Cancer Institute.

[‡] The coordinates for the structure of the recombinant hGSTM1a-1a enzyme have been deposited in the Brookhaven Protein Data Bank under file name 1GTU.

* To whom correspondence should be addressed. Telephone: (718) 430-2276. Fax: (718) 430-8565. E-mail: irving@aecom.yu.edu.

[1] Abbreviations: GST, glutathione *S*-transferase; GSH, glutathione; GS^-, glutathione thiolate anion; CDNB, 1-chloro-2,4-dinitrobenzene; CDNBA, 1-chloro-3,5-dinitrobenzoic acid; 3,4CDNB, 1-chloro-3,4-dinitrobenzene; DTT, dithiothreitol; EA, 2,3-dichloro-4-(2-methylenebutyryl)phenoxyacetic acid or ethacrynic acid; RT-PCR, reverse transcriptase polymerase chain reaction.

[2] For nomenclature of GSTs, see ref *12*.

10.1021/bi982164m CCC: $18.00
Published on Web 12/31/1998

supposition for different GSTs (*22*−*24*). However, a conserved tyrosine residue in the GSH binding domain (G-site) of GSTs (Y6 for Mu, Y7 for Pi, and Y8 for Alpha classes) was shown to be important for catalytic functions of the enzyme (*25*−*27*); the phenolic hydroxyl group is about 3.5 Å from the sulfhydryl group of GSH in protein−substrate complexes of different GSTs. The pK_a of that tyrosine is near 10 for class Mu GSTs, and not likely to abstract a proton directly from the sulfhydryl group, so that alternatively, it has been proposed that the tyrosine hydroxyl acts as a hydrogen bond donor to stabilize the deprotonated thiolate anion during catalysis (*20*).

Catalytic disparities among the class Mu GSTs are exemplified by differences between hGSTM1 and hGSTM4 subunit-containing enzymes. Thus, hGSTM4-4's sequence is 87% identical with that of hGSTM1-1, yet hGSTM1-1 is a much better catalyst with different substrates (*28*). Accordingly, in this report, hGSTM1 and hGSTM4 subunits were expressed in *Escherichia coli*, the crystal structure of a ligand-free hGSTM1a-1a was determined, and recombinant mutant proteins were designed to define a structural basis for the observed catalytic differences. A histidine residue at position 107 was shown to be crucial for the function of the enzyme.

MATERIALS AND METHODS

Materials. Substrates 1-chloro-2,4-dinitrobenzene (CDNB), 1,2-dichloro-4-nitrobenzene (DCNB), ethacrynic acid (EA), 4-chloro-3,5-dinitrobenzoic acid (CDNBA), and 1-chloro-3,4-dinitrobenzene (3,4CDNB) were purchased from Aldrich Chemical Co. (Milwaukee, WI). Reduced glutathione (GSH), *S*-methylglutathione, and GSH−agarose were purchased from Sigma Chemical Co. (St. Louis, MO).

Cloning, Expression, and Purification of Human Recombinant Class Mu GSTs. The nucleotide sequences encoding human hGSTM1a (an allelic variant, K172N) and hGSTM4 subunits were compared using BLAST and GENEPRO (version 4.10) programs for **nr** and **dbest** NCBI Genbank nucleotide sequence databases. On the basis of the alignment of cDNA sequences, the following specific primers were prepared: M1a sense, 5′-CCA ACC AGC CAT ATG CCC ATG ATA CTG GGG TAC-3′; M4 sense, 5′-CCA ACC AGC CAT ATG TCC ATG ACA CTG GGG TAC-3′ (each primer contained a restriction site for *Nde*I); and a common reverse primer for both hGSTM1a and hGSTM4, GCC TCC AGG ATC CTA CTT GTT GCC CCA GAC AGC CA, carrying a *Bam*HI restriction site (restriction sites are underlined). By using a QIAGEN purification kit, total RNA was purified from HeLa cells according to the manufacturer's instructions (QIAGEN Inc., Chatsworth, CA), and the cDNAs encoding corresponding GSTs were amplified using RT-PCR. The reverse oligonucleotide served as a primer for RAV-2 reverse transcriptase (Amersham Life Science Inc., Cleveland, OH), and synthetic cDNAs were added as templates in the PCR procedure [94 °C for 1 min, 55 °C for 1 min, and 72 °C for 1 min (35 cycles), and 2.5 units of Taq polymerase] in the manufacturer's buffer (Gibco BRL, Gaithersburg, MD). The purified PCR products were ligated into a *Nde*I−*Bam*HI restriction site of the pET3a expression vector (Stratagene, La Jolla, CA). The ligation mixture was then transformed into *E. coli* BL21(DE3) competent cells (Novagen, Madison, WI). Positive clones, which expressed recombinant GSTs, were identified by dot hybridization procedures by using peptide sequence-specific antisera raised against the different C-terminal segments of each subunit (*29*). Recombinant plasmid DNA was purified, and sequences were determined in both directions by using T7-Promoter and T7-Terminator primers in an Applied Biosystems automated sequencer (Perkin-Elmer Cetus, Emeryville, CA).

The fidelity of DNA sequencing procedures was confirmed by determination of molecular masses of resultant proteins using an API−III triple-quadrupole mass spectrometer (PE-SCIEX) as described by Rowe et al. (*16*). For example, the molecular masses measured for recombinant wild-type GST protein subunits, of GSTM1a [25 580 Da (*16*)] and of GSTM4 [25 430 Da (*16*)], were those deduced from their respective cDNA nucleotide sequences.

E. coli clones carrying recombinant plasmids were used for expression of recombinant GSTs as described previously (*30, 31*). The expressed proteins were purified by GSH affinity chromatography (*32*), and dialyzed against 10 mM Tris-HCl (pH 7.5) containing 0.2 mM DTT. The purity of the recombinant enzymes was tested under nondenaturing or denaturing conditions for gel electrophoresis in 12% polyacrylamide gels or by isoelectric focusing (pH 3−7, ready-to-use gels, NOVEX, San Diego, CA). GSTM1a−M4 chimeras were constructed by exploiting identical restriction sites in each of the cDNAs: *Bgl*II (at position 579 from ATG), *Nco*I (437), and *Pvu*II (331). An additional restriction site for *Nco*I (position 312) was identified in the cDNA for GSTM1a and was introduced into the cDNA for GSTM4 by genetic engineering methods. Site-directed mutagenesis was performed using PCR procedures and sets of site-specific primers. The resultant amplified fragments were subcloned into a pET3a vector and sequenced and GSTs expressed and purified as described above. Predicted protein primary structures were verified by ESI-MS. Affinity chromatography with GSH−agarose was used to purify all chimeric and wild-type GSTs.

Enzyme Assays. Unless otherwise stated, GST activities were determined in 0.1 M sodium phosphate buffer (pH 6.8) with 1.0 mM CDNB and 2.0 mM GSH as substrates. Initial reaction rates were monitored spectrophotometrically for 30−60 s via the increase of absorbance at 340 nm, and specific activities (micromoles per minute per milligram of protein) were calculated on the basis of the molar extinction coefficient for GS-DNB (9.6 mM^{-1} cm^{-1}) (*33*). Steady-state kinetic parameters were determined spectrophotometrically by using varying concentrations of GSH and other substrates independently in the ranges of 0.002−5.0 mM for GSH and 0.005−2.5 mM for the electrophilic substrate. The buffers used were 0.1 M sodium phosphate (or alternatively 0.1 M sodium acetate or 25 mM Tris-acetate) in the pH range between 4.0 and 9.0. Molar extinction coefficients of the different substrates used for calculations of enzyme activity were as follows: $\epsilon = 9.0$ mM^{-1} cm^{-1} (340 nm) for CDNBA, $\epsilon = 5.6$ mM^{-1} cm^{-1} (370 nm) for 3,4CDNB, and $\epsilon = 5.0$ mM^{-1} cm^{-1} (270 nm) for EA (*28*). The apparent kinetic constants k_{cat}, K_m^S, and K_m^{GSH} for each recombinant protein with the different substrates were calculated from plots of initial velocities $1/v_o$ versus 1/[S]; a Milton Roy Co. (Rochester, NY) Software kinetics program package was used. If we assume that the Michaelis constant for each

substrate is identical to its dissociation constant, all kinetic data were consistent with steady-state random equilibrium or random sequential bi-bi rate equations. Inhibitors were tested at various concentrations of GSH and CDNB, and K_i values were calculated from Michaelis−Menten equations for competitive, noncompetitive, or mixed-type inhibition mechanisms.

Enzyme concentrations were determined spectrophotometrically at 280 nm and by using a Bio-Rad Protein Assay colorimetric solution according to the manufacturer's manual (Bio-Rad Laboratories, Hercules, CA). The k_{cat} values for each substrate were recalculated on a per-GST subunit basis. All measurements were made in triplicate in buffers equilibrated at ambient temperature.

Rapid kinetic rate constants for CDNBA and 3,4CDNB as substrates were also determined by stopped-flow spectrophotometry by using an Applied Photophysics SX-17MV spectrophotometer. Each reaction was performed after rapid mixing of two solutions with mixing times of about 1 ms. The first syringe contained the mixture of protein (4 μM) and 1.0 mM GSH in 0.1 M sodium phosphate buffer (pH varied between 6.0 and 8.0), and a second syringe contained the indicated hydrophobic substrate at 0.08−1.0 mM in the same buffer. Rate constants calculated from the transient-state kinetic experimental data were consistent with those obtained from the routine steady-state spectrophotometric analysis described above. Rate constants for uncatalyzed nonenzymatic reactions were determined for each substrate according to a previously reported method (*34*). The pH dependence of k_{cat} and k_{cat}/K_m was analyzed according to relationships described by Cleland (*35*).

Thiolate Formation. The extent of thiolate formation was determined spectrophotometrically using a Kontron Uvicon 9420 spectrophotometer by measuring the absorbance at 239 nm (*19*). An appropriate amount of GSH was added to the buffer solution that contained protein at a fixed concentration of 20 μM (calculated per monomer). Solutions of GSH alone and of protein alone at the same concentrations were used as blanks. Each measurement was made at least in triplicate. A molar extinction coefficient of 5.2×10^3 M^{-1} cm^{-1} (*19*) was used for calculation of molar ratios of enzyme and thiolate. The maximum increase of absorbance at 239 nm was plotted versus GSH concentration to reflect the concentration of the protein−thiolate complex. To determine the apparent pK_a of enzyme-bound GSH, the maximal increases of absorbance at 239 nm were determined as a function of pH.

Fluorescence Titration of GSH Binding. Binding constants for GSH and *S*-methylglutathione (K_d) were determined from changes in intrinsic fluorescence (excitation wavelengths of 280 and 295 nm and emission wavelength of 340 nm). GSH concentrations were varied from 0.5 to 1000 μM at a fixed protein concentration (4 or 10 μM). A similar protocol was used for analysis of *S*-methylglutathione binding. All measurements were performed in 0.1 M sodium phosphate buffer at pH 6.5 by using a Perkin-Elmer LS-5 fluorometer with a thermostated sample holder at 25 °C. Ligand binding affinities were determined from measurement of intrinsic fluorescence quenching, which were corrected for nonspecific quenching obtained at high GSH concentrations. The data were analyzed using the Stern−Volmer, Scatchard, and Hill equations (*36*). Affinity constants were obtained from slopes of Scatchard plots.

Crystallization of hGSTM1a-1a. Crystals of ligand-free GST (see ref *30*) were grown by the hanging drop vapor diffusion method. To select optimal conditions for obtaining crystals, the Hampton Crystal Screen Kit (Hampton Research Inc., Laguna Hills, CA) was used. Variations of buffer conditions were tested to improve the quality of crystals and to increase their size. In the final step, recombinant hGSTM1a-1a (16−20 mg/mL) in 10 mM Tris-HCl (pH 7.5) and 0.2 mM DTT was equilibrated against 16−22% PEG 4000 in buffer containing 50 mM KH_2PO_4 and 25 mM Tris-HCl (pH 6.0). All procedures were performed at 289 K. The largest crystals with average lengths of 0.4−1 mm were chosen for X-ray analysis.

X-ray Data Collection. Diffraction data to 2.7 Å resolution were collected and reduced with XDS (*37*) at ambient temperature using a Rigaku RU-200 rotating anode X-ray source operating at 50 kV and 80 mA, coupled to a Siemens X-1000 multiwire area detector. A total of 26 217 independent reflections were collected with an overall R_{merge} of 5.8%. Analysis of the data integrated at low-symmetry space group *P*1 showed that the pattern of systematically absent reflections was consistent with space group $P2_12_12_1$. The unit cell volume was compatible with four monomers in the asymmetric unit with a V_m (volume/protein molecular weight) (*38*) value of 2.87 $Å^3$ and a water content of about 58%.

Solution of the hGSTM1a-1a Crystal Structure, Model Building, and Refinement. The three-dimensional structure of hGSTM1a was solved by molecular replacement techniques, using X-PLOR software (*39*), parameters for energy and stereochemistry (*40*), and the structure of GSTM2 (PDB entry 2GTU) refined to 2.55 Å (*30*). Because of the high degree of amino acid sequence identity (86%) between the hGSTM2 and hGSTM1a subunits, similar tertiary and/or quaternary structures for these two enzymes were expected. The cross rotation function was calculated in the range of 10.0−4.0 Å and provided large groups of rotation peaks with correlation coefficients that varied from 6.0 to 5.0. The 50 highest peaks were applied for PC refinement to identify the four largest peaks (correlation coefficients of 8.0−11.0). The analysis by Rotman-statement provided evidence that these four peaks may be divided in two groups of rotation matrixes in which one group is located far from the other. On the basis of the assumption that each GST is a dimer, it was likely that an asymmetric unit carries two dimers rather than four monomers. The translation search for each rotation matrix gave a solution with correlation coefficients that varied between 14.0 and 18.0. A combined translation function was applied to determine the relative positions among four monomers. The final model was subjected to rigid-body refinement (resolution range of 10.0−4.0 Å) that provided an *R*-factor of 0.38 (*R*-free of 0.45) and appeared to favor a combination of two dimeric molecules per asymmetric unit. Several additional cycles of refinement were used to improve the quality of the model. The progress of refinement was always monitored using cross validation methods. Operations that lowered *R*-free values were those applied for refinement. The final model contains two homodimeric protein molecules per asymmetric unit. The crystallographic *R*-factor for 23 012 reflections between 10.0 and 2.7 Å with $F > 2\sigma$ is 0.21 (*R*-free is 0.245) with root-mean-square deviations in bond lengths and angles being 0.012 and 1.32 Å, respectively. Water molecules associated

```
                  10        20        30        40        50
hGSTM1a     PMILGYWDIRGLAHAIRLLLEYTDSSYEEKKYTMGDAPDYDRSQWLNEKFKLGLDFPNL
hGSTM4      S-T-------------------------------------------------------

            60        70        80        90        100       110
hMGST1a     PYLIDGAHKITQSNAILCYIARKHNLCGETEEEKIRVDILENQTMDNHMQLGMICYNPEF
hGSTM4      ----------------------------------------A--VSN--ARV--S-D-

            120       130       140       150       160       170
hGSTM1a     EKLKPKYLEELPEKLKLYSEFLGKRPWFAGNKITFVDFLVYDVLDLHRIFEPKCLDAFPN
hGSTM4      -----E------TMMQHF-Q--------V-D--------A-----------N-------

            180       190       200       210
hGSTM1a     LKDFISRFEGLEKISAYMKSSRFLPRPVFSKMAVWGNK
hGSTM4      ------------------------K-LYTRV------
```

FIGURE 1: Sequence alignment of hGSTM1a and hGSTM4 subunits. Residues that are identical to those of hGSM1a are represented by dashes.

with difference electron density in excess of 4σ and consistent with hydrogen bonding were added to the model. Experimental details of this structural solution and data collection and refinement statistics were submitted to the Brookhaven Protein Data Bank (entry 1GTU). All models were built using a Silicon Graphics workstation, the software TOM (*41*), and the INSIGHTII program package (Biosym Inc.). In this report, the hGSTM1a monomer A structure is presented as a model of the GSH-binding site.

RESULTS

Domain Swapping between hGSTM1a and hGSTM4 Subunits. The amino acid sequences of hGSTM1 and hGSTM4 subunits are 87% identical (Figure 1), yet hGSTM4-4 is generally much less effective in catalyzing nucleophilic aromatic substitution reactions as compared to hGSTM1-1 (*28*). To establish a structural basis for the observed catalytic differences and to determine whether the catalytic mechanisms of these two GST isoforms differ, a series of chimeric hGSTM1a−M4 enzymes were designed and constructed. Their N termini extending through residue 106, which contain the GSH binding domains (G-sites), are virtually identical except for three amino acid substitutions. The sequence divergence between these subunits is primarily located between residues 106 and 113, 131 and 136, and six substitutions of the seven residues at positions 204−210, which is part of the H-site (Figure 1). These three regions were considered likely to account for the wide disparity in catalytic efficiencies of hGSTM1-1 and hGSTM4-4, and thus were targeted for design of chimera with reciprocal modular and site-directed mutations.

Initially, specific activities of the recombinant enzymes were surveyed with CDNB, which is widely used as a substrate for spectrophotometric assays of GSTs (*33*). Under standard assay conditions, the wild-type hGSTM1a-1a had an about 50-fold greater activity than hGSTM4-4 (Figure 2). Reciprocal interchange of the C-terminal domains had little effect on enzyme activities, even though their C termini are sufficiently different that peptide sequence-specific antisera discriminate between the two subunits (*16*, *29*). In fact, the entire regions that encompass 140 residues to the C terminus may be interchanged between hGTM1a-1a and hGSTM4-4 without substantially affecting catalytic activities (Figure 2). Evidently, large segments of the protein may be exchanged without disrupting the overall protein fold or the

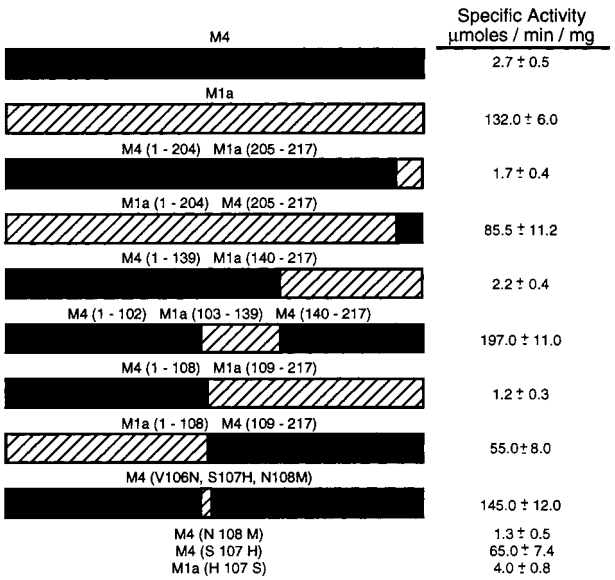

FIGURE 2: Schematic representation of engineered hGSTM1a−GSTM4 chimeric and mutant enzymes and their specific activities with CDNB and GSH as substrates. The solid bars represent hGSTM4 sequences, and the hatched bars are those of hGSTM1a. Enzyme activities were determined with 1.0 mM GSH and 1.0 mM CDNB as substrates at pH 6.5 as described in Materials and Methods.

integrity of the catalytic site. The specific activity of a double-reciprocal chimera, $hGSTM4_{1-102}M1a_{103-139}M4_{140-217}$, however, was 70-fold greater (197 μmol min^{-1} mg^{-1}) than that of the wild-type hGSTM4-4. The relatively large protein segment responsible for such differences (residues 103−139) was further narrowed by construction of two other types of reciprocal chimeras, $hGSTM4_{1-108}M1a_{109-217}$ and $hGSTM1a_{1-108}M4_{109-217}$ (Figure 2). Comparison of specific activities for these two chimeric enzymes as well as others shown in Figure 2 suggest that residues 106−108 could account for the differences between hGSTM1a-1a and hGSTM4-4. These three residues in hGSTM4 (Val-Ser-Asn) were accordingly replaced with the corresponding residues of hGSTM1a (Asn-His-Met) (see Figure 1). The resultant triple mutant hGSTM4-4(V106N/S107H/N108M) had a much higher specific activity with CDNB as a substrate (145 μmol min^{-1} mg^{-1}) as compared to the wild-type hGSTM4-4 protein (2.8 μmol min^{-1} mg^{-1}). A single-point mutation N108M in hGSTM4 had no significant effect on catalytic rates, which remained comparable to those of the wild-type

Table 1: Apparent Steady-State Kinetic Constants for Wild-Type and Mutant GSTs with Different Substrates (pH 6.2)[a]

protein	substrate	K_m^S (mM)	K_m^{GSH} (mM)	k_{cat} (s^{-1})	k_{cat}/K_m^S (s^{-1} mM^{-1})	k_{cat}/K_m^{GSH}
hGSTM1a-1a	CDNB	0.31 ± 0.05	0.14 ± 0.03	24.7 ± 2.1	79.7	176.4
	CDNBA	0.01 ± 0.003	0.17 ± 0.04	0.05 ± 0.02	5.0	0.3
	3,4CDNB	1.8 ± 0.5	0.15 ± 0.04	1.7 ± 0.3	0.9	1.1
	EA	0.015 ± 0.005	0.20 ± 0.05	0.08 ± 0.03	5.3	0.25
M1a(H107S)	CDNB	0.8 ± 0.2	0.20 ± 0.05	0.7 ± 0.1	0.9	3.5
	CDNBA	0.02 ± 0.005	0.20 ± 0.04	0.0008	0.04	0.004
	3,4CDNB	1.8 ± 0.5	0.19 ± 0.04	0.06 ± 0.02	0.03	0.32
	EA	0.02 ± 0.005	0.2 ± 0.06	0.04 ± 0.03	2.0	0.2
M1a(Y6F)	CDNB	0.25 ± 0.04	0.15 ± 0.03	0.8 ± 0.2	3.2	5.3
	CDNBA	0.015 ± 0.004	0.11 ± 0.03	0.001	0.07	0.009
	3,4CDNB	2.0 ± 0.8	0.20 ± 0.05	0.003	0.015	0.15
	EA	0.012 ± 0.004	0.18 ± 0.03	0.03 ± 0.01	2.5	0.17
M1a(Y6F/H107S)	CDNB	0.7 ± 0.1	0.26 ± 0.04	0.04 ± 0.01	0.06	0.15
hGSTM4-4	CDNB	1.6 ± 0.3	0.40 ± 0.05	0.25 ± 0.04	0.16	0.63
	CDNBA	0.04 ± 0.005	0.40 ± 0.04	0.001	0.025	0.0025
	3,4CDNB	1.7 ± 0.5	0.40 ± 0.06	0.04 ± 0.02	0.023	0.1
	EA	0.035 ± 0.005	0.45 ± 0.05	006 ± 0.03	1.7	0.13
M4(S107H)	CDNB	0.8 ± 0.2	0.50 ± 0.10	20.8 ± 2.3	26	41.6
	CDNBA	0.04 ± 0.008	0.40 ± 0.04	0.04	1.0	0.1
	3,4CDNB	1.8 ± 0.6	0.50 ± 0.07	1.6 ± 0.2	0.9	3.2
	EA	0.038 ± 0.005	0.40 ± 0.05	0.15 ± 0.03	3.9	0.4
M4(Y6F)	CDNB	2.4 ± 0.8	0.46 ± 0.07	0.04 ± 0.01	0.017	0.09

[a] K_m^S, where S is any of the indicated substrates other than GSH. All kinetic data were consistent with random sequential or random equilibrium bi-bi reaction mechanisms.

GSTM4-4 (Figure 2). Of these three residues, the only single-point mutant of hGSTM4 that substantially increased the enzymatic activity was S107H. Conversely, a hGSTM1a-(H107S) mutant retained only about 3% of the activity (4 μmol min^{-1} mg^{-1}) of the wild-type hGSTM1a-1a enzyme. On the basis of these results, it was reasonable to assume that the nature of the side chain of residue 107 is important for catalytic activity, and the presence of serine at position 107 instead of a histidine could be responsible for the relatively low specific activities of hGSTM4-4 with many different substrates (*28*).

Because tyrosine 6 has been reported to be essential for GST catalysis by the rat rGSTM1-1 (*25*) and human hGSTM2-2 enzymes (*42*), enzymes with single-point mutations of hGSTM1a(Y6F) and hGSTM4(Y6F) were also engineered, and their catalytic properties were compared to those of the corresponding wild-type enzymes. In contrast to the rat class Mu enzyme on which the Y6F mutant retained only about 1.0% of its activity (*25*), lesser effects were observed for these human GSTs (hGSTM1a and hGSTM4), and the Y6F mutation had very small effects on catalysis of the nucleophilic addition reaction to ethacrynic acid (Table 1).

Kinetic Properties of Wild-Type and Mutant GSTs with Different Substrates. To underscore the function of residue 107 in catalysis, kinetic properties of wild-type hGSTM1a-1a and hGSTM4-4 and single reciprocal mutants hGSTM1a-(H107S) and hGSTM4(S107H) were compared with those of different substrates. Data determined by steady-state kinetic analysis are presented in Table 1. Pre-steady-state kinetic data were also obtained by rapid mixing stopped-flow spectrophotometry with CDNBA and 2,3CDNB as substrates. Single-turnover bursts were not evident, and the kinetic data were identical to those obtained by steady-state analysis with these substrates. Moreover, there were no changes in steady-state kinetic parameters for hGSTM1a-1a and for the hGSTM4-4(S107H) mutant as a function of viscosity in solutions of up to 30% sucrose. These results suggest that diffusion-limited steps are not rate-limiting in catalysis with these substrates.

Table 2: Binding Constants for Binding of GSH and *S*-Methylglutathione to Wild-Type and Mutant Enzymes[a]

ligand	K_d (μM) hGSTM1a	hGSTM1a-(H107S)	hGSTM4	hGSTM4-(S107H)
GSH	2.4 ± 0.5	1.6 ± 0.6	1.4 ± 0.7	2.0 ± 0.5
S-methyl-GSH	2.5 ± 0.7	2.0 ± 0.5	2.2 ± 0.6	2.5 ± 0.8

[a] The degree of binding was determined by fluorescence quenching methods as described in Figure 3 and Materials and Methods.

His107 is responsible for the 100-fold greater turnover number of hGSTM1a-1a as compared to hGSTM4-4 with CDNB as a substrate, and for increased turnover numbers with related nitrobenzene derivatives (Table 1). By contrast, K_m values determined for the aromatic substrates were relatively independent of whether wild-type enzymes or H107S or even Y6F mutant forms were employed. It is noteworthy that K_m^{GSH} values were nearly identical for all substrate reactions, and were also similar to K_i values determined for these reactions using the competitive inhibitor *S*-methylglutathione (K_i of 115 ± 20 μM). There were no strong correlations between K_m values determined for the different electrophilic substrates and rate constants measured for the same compounds.

Binding of GSH and S-Methylglutathione. The Trp7 and Trp45 residues that are highly conserved among all class Mu GSTs, including the human proteins, are in part involved in GSH binding (*20*, *43*−*45*). The proximity of these tryptophan residues to the bound GSH provides a means for determining GSH binding constants by fluorescence quenching methods. Dissociation constants for both GSH (K_d^{GSH}) and *S*-methylglutathione (K_d^{GSMe}) were almost 100-fold lower (approximately 2 ± 1 μM) (Table 2) than the apparent K_m^{GSH} values calculated from kinetic data (Table 1). Moreover, the GSH binding constants for each of the mutated GSTs shown

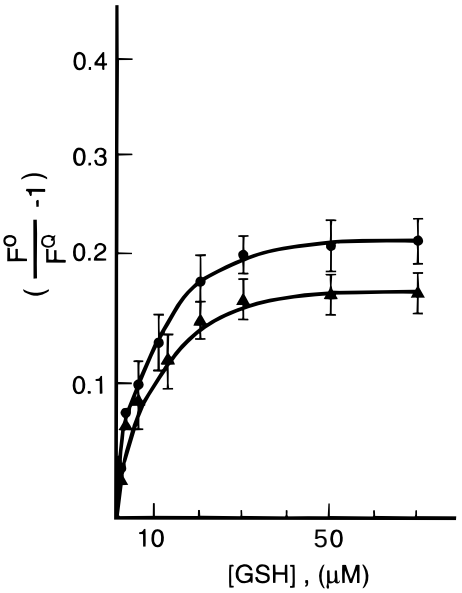

FIGURE 3: Binding of GSH and *S*-methylglutathione to hGSTM1a-1a. The extents of GSH (●) and *S*-methylglutathione (▲) binding to hGSTM1a-1a were determined by fluorescence quenching methods (excitation at 280 nm and emission at 340 nm). Dissociation constants (K_d) were obtained by measurement of changes in intrinsic fluorescence using the Stern−Volmer relationship $F_o/F_Q - 1$, where F_o is the intrinsic fluorescence in the absence of ligand and F_Q is the quenched fluorescence. The protein concentrations were 4 μM for these experiments.

Table 3: Rate Constants and pH Dependence of Nonenzymatic Reactions of GSH with Various Compounds

compound	k_s (s^{-1} M^{-1})[a]	pK_a
CDNB	2.2 ± 0.3	8.7 ± 0.2
CDNBA	0.7 ± 0.3	9.0 ± 0.2
3,4CDNB	0.9 ± 0.3	9.2 ± 0.1
EA	257 ± 26	9.0 ± 0.3

[a] Rate constants were determined at pH 9.0.

in Figure 2 were similar to those obtained with the wild-type enzymes. Data analysis by the Stern−Volmer relationship (Figure 3) showed ligand saturation of approximately 1 mol per subunit with a Hill coefficient of −1.0, indicating an apparent lack of cooperativity between sites with independent ligand binding at each subunit of the dimer. Similar results were obtained with corresponding Y6F mutants.

pH Dependence of Nonenzymatic Reactions. The rates of nonenzymatic nucleophilic substitution and addition reactions of GSH were pH-dependent for the compounds used as substrates in this study. The pK_a values determined for the spontaneous reactions (Table 3) were 8.7−9.2, which is close to the pK_a of GSH thiolate formation as determined by spectrophotometric titrations. For the nonenzymatic reactions, all nitrobenzene derivatives studied had similar values of second-order rate constants. However, the nucleophilic addition of GSH to ethacrynic acid (EA) occurred at a rate that was at least 100-fold faster than that of the nucleophilic aromatic substitution reactions with the other substrates (Table 3).

pH Dependence of Enzymatic Reactions. The rates of the enzymatic reactions also varied as a function of pH, but K_m^{GSH} did not vary significantly over this pH range. Examples of the pH dependence of k_{cat} for the catalytic conjugation reactions of GSH with CDNB as a substrate are illustrated in Figure 4. Apparent pK_a values for hGSTM1a-1a could not be determined directly from plots of log k_{cat} versus pH, since the slopes were much less than 1 over the accessible pH range examined (Figure 4A). By contrast, for the same data for a hGSTM1a-1a(H107S) mutant within the pH range of 6.0−8.0, an ionization with an apparent of pK_a of 7.6 ± 0.2 separates two forms of the enzyme with k_{cat} values which differ by a factor of about 100 at pH values below 6.5. The hGSTM4-4 and hGSTM1a-1a(H107S) enzymes displayed similar pH dependencies for catalysis with apparent pK_a values between 7.5 and 7.9 ± 0.2 (Figure 4B). Likewise, a plot of log k_{cat} versus pH for the hGSTM4-4(S107H) mutant (Figure 4B) was very similar to that of wild-type hGSTM1a-1a. Y6F substitutions had little effect on the pH profiles of both hGSTM1a-1a and hGSTM4-4 (Figure 4A,B).

The distinct effect of the H107S substitution could be deduced from differential plots of Δlog k_{cat} versus pH (Figure 4C) in which slopes of −1 clearly indicated an ionization with a pK_a of about 6.2 which can be directly attributed to the His107 residue. These results reinforce the notion that His107 could serve as a general base in GST catalysis. Significantly, the differences between k_{cat}^{lim} values exhibited by wild-type and mutant enzymes converged at more basic pH values above 8.0. In general, the apparent pK_a values derived from plots of log k_{cat}/K_m(CDNB) versus pH were 6.3−6.5 for hGSTM1a-1a and hGSTM4-4(S107H) and about 7.8 for hGSTM1a-1a(H107S) and hGSTM4-4 (Figure 4D).

Detectable levels of GST activity were observed for all enzymes with all substrates over a pH range of 4.5−9.5. In all cases, K_m^{GSH} values were largely pH-independent so that relationships of log k_{cat} versus pH are almost identical to those of log k_{cat}/K_m^{GSH} versus pH. However, the K_m^S values determined for each electrophilic substrate decreased until a k_{cat}^{lim} was reached. The pH profiles of enzyme activity as well as apparent pK_a values of catalysis, calculated from plots of log k_{cat}/K_m^S versus pH for CDNBA and 3,4CDNB as substrates, were similar to those obtained for CDNB (data not shown).

The apparent pK_a values determined for ethacrynic acid as a substrate were distinct and much lower than those for other substrates. With EA as a substrate, the following apparent pK_a values of catalysis were obtained: 5.0 ± 0.4 for hGSTM1a-1a, 5.0 ± 0.4 for hGSTM1a(H107S), 6.2 ± 0.3 for hGSTM4-4, and 6.3 ± 0.3 for hGSTM4(S107H). Apparently, the H107S substitution had only a moderate effect on this type of catalyzed nucleophilic addition reaction (see Table 1).

Thiolate Formation. On the basis of the results of the nucleophilic aromatic substitution reactions, it was considered likely that the His107 residue lowers the pK_a for the GSH-thiol group after that substrate binds to the enzyme. Direct determination of enzyme-bound thiolate anion by spectrophotometric titrations (differential absorbance at 239 nm) showed a clear dependence on the presence of a His side chain in position 107 (Figure 5A). Thus, the apparent pK_a values of bound GSH calculated for hGSTM1a-1a, hGSTM1a-1a(Y6F), and hGSTM4-4(S107H) were estimated to be about 6.6 ± 0.3, which is in close agreement with the lower apparent pK_a values of the GSH sulfhydryl group complexed with other GSTs (*20*). It is noteworthy, however, that binding to hGSTM4-4 and hGSTM1a-1a(H107S) produced relatively

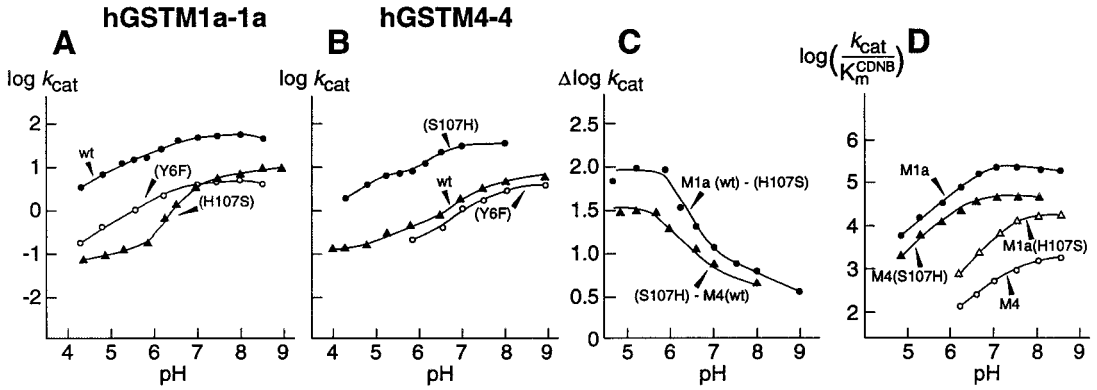

FIGURE 4: pH dependence of the activity of wild-type and mutant enzymes. (A) pH dependence of log k_{cat} for hGSTM1a-1a (●), hGSTM1a-1a(H107S) (▲), and hGSTM1a-1a(Y6F) (○) with CDNB as a substrate. (B) pH dependence of log k_{cat} for hGSTM4 (▲), hGSTM4-4(S107H) (●), and hGSTM4-4(Y6F) (○) with CDNB as a substrate. (C) The effects of H107S substitutions. The differences obtained by subtraction of log k_{cat} of wild-type hGSTM1a minus that of GSTM1(H107S) (●) and for that of mutant hGSTM4(S107H) minus that of wild-type hGSTM4 (▲) are shown to resolve the influence of His107 on the pH profile. (D) pH dependence of log k_{cat}/K_m^{CDNB} for hGSTM1a (●), hGSTM1a(H107S) (△), hGSTM4 (○), and hGSTM4(S107H) (▲).

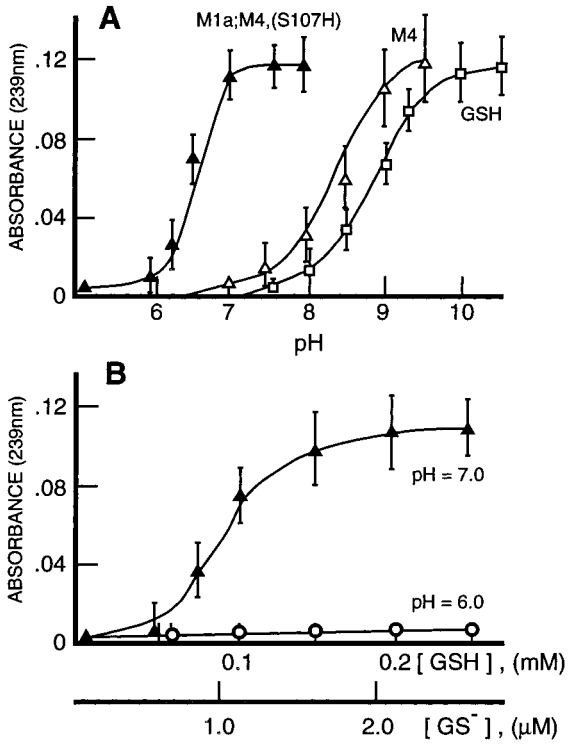

FIGURE 5: GST-dependent GSH thiolate anion formation as a function of pH. (A) The hGSTM1a-1a (▲) and hGSTM4-4 (△) protein concentrations were 20 μM, and GSH was at saturating concentrations of 400 and 600 μM, respectively. A control titration for GSH in the absence of GST (□) at a concentration 20 μM reflects a pK_a value of about 8.7 for enzyme-independent deprotonation of GSH. (B) GST-dependent thiolate formation as a function of GSH concentration. Data are shown for GSTM1a-1a (20 μM) at pH 6.0 (○) and 7.0 (▲). The equilibrium concentration of thiolate anion in solution at pH 7.0 (abscissa) was estimated on the basis of the pK_a of GSH. The half-saturation GSH concentration was estimated to be 90 ± 20 μM.

small shifts of pK_a relative to that of free GSH from 8.7 ± 0.3 to approximately 8.0 ± 0.3.

The formation of GSH-thiolate after binding to the enzyme not only depends on pH but also depends on GSH concentration at equilibrium (Figure 5B). In these experiments, the protein concentration per active site was about 20 μM (Figure 5B); thus, the increase in absorbance at 239 nm (0.1A ± 0.02) at saturation was consistent with a completely deprotonated (GS^-) ligand bound to each subunit at a GSH:protein molar ratio of 1.05 ± 0.25:1 or a stoichiometry of one thiolate binding site per subunit. However, on the basis of these data, the apparent dissociation constants for GSH-thiolate binding to the enzyme were near 10^{-4} M; this value is almost 100-fold greater than those determined for GSH binding from fluorescence quenching data (Figure 3), but close to the K_m^{GSH} constant determined from steady-state kinetics (Table 1). However, at equilibrium, the concentration of thiolate anion (GS^-) in solution at pH 7.0 is almost 100-fold lower than that of the protonated form (pK_a = 8.9). On this basis, the affinity of thiolate binding to the enzyme (Figure 5B) is virtually identical to that of protonated GSH (Figure 3).

Three-Dimensional Structure of GSTM1a. In view of amino acid sequence identities between hGSTM1a and hGSTM2 subunits (85%), it is likely that the two proteins are structurally similar. The structure of a ligand-free hGSTM1a-1a determined here was compared to that of hGSTM2-2 (*30*) and hGSTM2-2 complexed with GSH (*46*). Between backbone atoms in these two structures, rms deviations were found to be about 0.6 Å. However, between residues around and at the GSH-binding site, rms deviations were only 0.2 Å, and were comparable for the ligand-free enzyme and those complexed with GSH derivatives. Residues directly involved in the binding of GSH are also identical in these enzymes. These considerations and ligand-free structural information allowed modeling of the GSH−hGSTM1a-1a complex based on hGSTM2-2. In the model, GSH is anchored to the protein by as many as 12 hydrogen bonds and electrostatic interactions provided mainly by side chains of residues Tyr6, Trp7, Arg42, Trp45, Lys49, Asn58, Leu59, Gln71, Ser72, and Asp105 (second protein subunit) which are conserved in all class Mu GSTs (*3*, *20*). The closest distance between the imidazole nitrogens of the His107 side chain and the sulfur atom of GSH is about 6.0 ± 0.5 Å, which is greater than the hydrogen bond distance even for S−H interactions (3−3.5 Å) (Figure 6A). However, this histidine residue is much closer to the GSH than any other His residues of the hGSTM1a-1a or of other class Mu GSTs (*20*, *43*−*45*). Figure 6B shows that the His107 residue is in a hydrophobic region that lines the ligand binding pocket and is oriented toward the crevice.

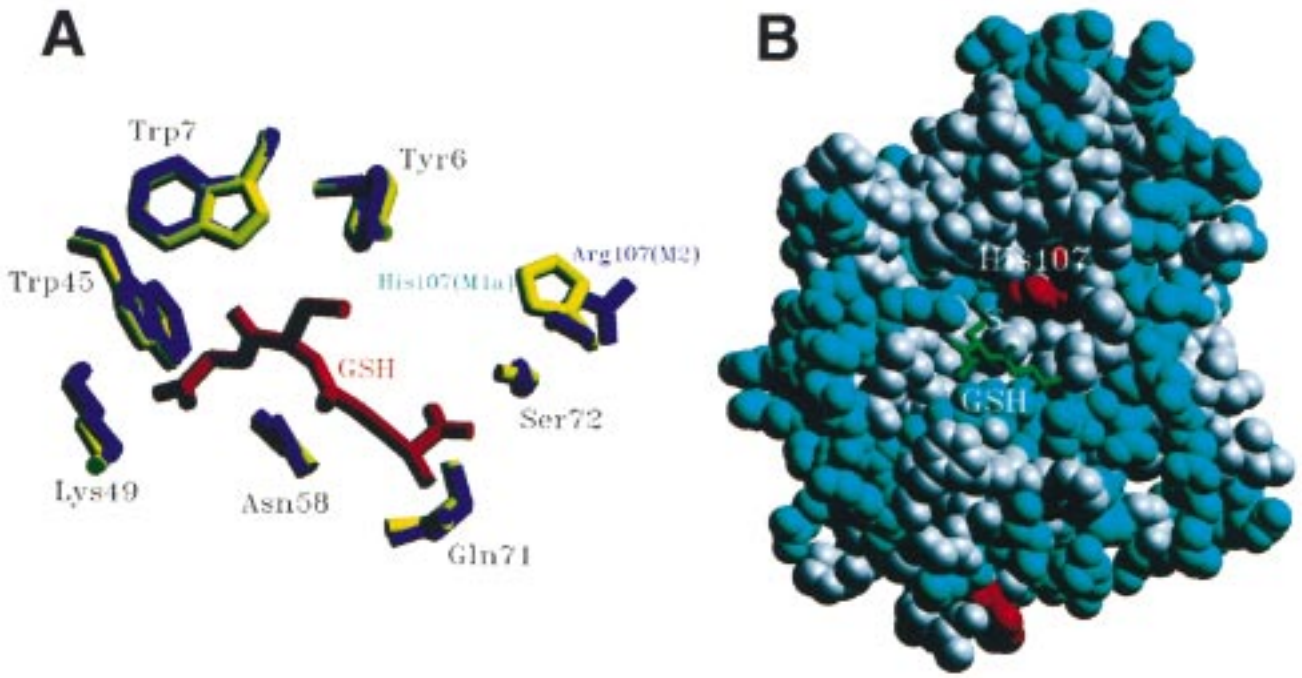

FIGURE 6: GSH binding site of a hGSTM1a subunit. (A) Some of the key residues involved in GSH binding are labeled in this representation. The yellow residues are those of the hGSTM1a subunit, and the corresponding residues of hGSTM2 are superimposed in blue. The orientation of the His107 residue of hGSTM1a and that of the corresponding R107 of hGSTM2 are shown for comparison. The bound GSH is red. (B) Space-filling van der Waals sphere interaction model of the surface of the hGSTM1a subunit (hydrogen atoms not shown). The catalytic cleft is visible from this representation of a monomeric hGSTM1a subunit. The color coding depicts hydrophilic residues in blue and the more hydrophobic residues in gray. Histidine residue 107 is red in the hydrophobic pocket, and bound GSH with the sulfur atom labeled is green.

DISCUSSION

The catalytic mechanism of hGSTM1a-1a is exceptional for GSTs because of the involvement of a histidine residue near the active site pocket. Thus, a H107S substitution alone accounts for the pronounced differences between hGSTM1a-1a and hGSTM4-4 in their ability to catalyze nucleophilic aromatic substitution reactions (Table 1); hGSTM1a-1a containing a His107 is a much more effective enzyme than its homologue hGSTM4-4 which has a serine residue at that position. This notion was confirmed by studies of reciprocal mutants (Table 1 and Figure 4), where the catalytic properties of hGSTM4-4 and hGSTM1a-1a could be interconverted by the single S107H mutation.

By analogy to cysteine proteases in which an active site cysteine interacts with a nearby histidine residue to form a thiolate−imidazolium ion pair (*47*), it seems plausible that at physiological pH values, a histidine residue of GSTs could be involved in thiolate anion formation of enzyme-bound GSH. In structures determined for cytosolic GSTs (including Alpha, Mu, and Pi classes), no histidine residue is located closer than 8−10 Å from the putative catalytic pockets (*43*−*45*, *48*). Moreover, chemical modification, or site-directed replacement of all histidine residues by asparagine residues in rat GSTM1-1 (*22*) or in human GSTP1-1 (*23*), did not affect catalytic activities of the modified proteins. The conserved His14 of hGSTM1-1 was postulated to have a structural role rather than a role as a specific or general base in catalysis. Indeed, the crystal structure of hGSTM1a-1a indicates that His14 is more than 8 Å distant from the catalytic pocket. It may be noted that recent crystal structures of bacterial GSTs (*49*, *50*) revealed histidine residues in close proximity to sulfur atoms of bound GSH. Until now, however, there had been no evidence for direct involvement of histidine residues in catalytic activity of GSTs.

The effects of His107 on GST catalysis are mainly reflected by the pH dependence of catalytic activities (or k_{cat}/K_m) with CDNB as a substrate; thus, an ionization state at a pK_a of about 6.3 was obtained for the enzymes containing His107 with a shift to 7.8 for the H107S mutants (Figure 4). That shift in pK_a is directly attributed to the His107 residue (Figure 4C) and parallels the apparent pK_a for formation of thiolate anion of GSH bound to the corresponding enzymes (Figure 5). These results indicate that in this case the nature of residue 107 determines the chemical reaction mechanism in GST catalysis. Substantial involvement of either His107, or for that matter Ser107, in substrate binding is not likely because the H107S substitution had no effect on GSH binding properties (Tables 1 and 2). Also, no significant differences in kinetic constants, with the exception of increases in turnover numbers (Table 1), could be correlated with the presence of His107 for all substrates tested. It is likely, therefore, that His107 is involved in the activation of the GSH nucleophile. In fact, the pK_a's of the thiol group of GSH bound to wild-type hGSTM4-4 or the hGSTM1a-1a(H107S) mutant are not substantially lower than the pK_a of free GSH in solution.

Evidently, the thiolate anion is the activated form of GSH bound to the His107-containing enzymes, and its relatively enhanced nucleophilicity is important for catalysis of nucleophilic aromatic substitution reactions. Mechanisms that have been proposed for other GSTs in which the Tyr6 hydroxyl group acts as a hydrogen bond donor to stabilize

the thiolate anion (*19*) seem to be less important for the His107-containing enzymes since Y6F mutated forms show almost no changes in the pH profiles. For the rat rGSTM1-1 enzyme, it has also been suggested that an on-face hydrogen bond between the Thr13 hydroxyl group and the π-electrons the Tyr6 ring increases the hydrogen bond strength to stabilize the thiolate (*51*). In fact, a T13A mutant for rGSTM1-1 increased the apparent pK_a of the enzyme-bound GSH thiol by 0.7 log unit (*51*). In this context, it is noteworthy, therefore, that **all** of the known human class Mu GSTs have an alanine residue at position 13.

Binding affinities of GSH for hGSTM1a-1a and hGSTM4-4, and for the M1a−M4 chimera, are very similar, with dissociation constants near 2×10^{-6} M (Table 2). The K_d values for both GSH and *S*-methyl-GSH are almost identical, indicating that formation of thiolate anion is not a requisite for GSH binding to these enzymes. According to their respective pK_a values for His107-containing enzymes, the ratio of thiolate anion to protonated GSH ([GS^-]/[GSH]) of the protein-bound ligand at equilibrium (pK_a = 6.3−6.4) should be approximately 300-fold greater than that ratio in solution (pK_a = 8.9); the equilibrium at pH 7.0 therefore lies in favor of the bound thiolate anion. Equilibrium studies by direct spectrophotometric measurement of thiolate anion binding at pH 7.0 for the His107 enzymes as a function of GSH concentration (Figure 5B) yielded apparent dissociation constants that were approximately 100-fold higher (K_d near 10^{-4} M) than those determined by flourescence quenching. Those values are close to the K_m^{GSH} values determined by steady-state kinetics, and the K_i values for *S*-methyl-GSH inhibition with various substrates (0.1−0.4 mM). However, at pH 7.0, the GSH thiolate anion concentration present in solution is, in fact, approximately 100-fold lower than that of the protonated GSH (Figure 3B). On that basis, the apparent affinities for binding of GSH and GS^- are virtually the same. The fact that these values are 100-fold lower than the K_m^{GSH} values suggests that the ionization step for forming enzyme-bound thiolate is fast relative to GSH release. Moreover, if the thiolate anion of GSH is considered to be the activated form of that compound in the Michaelis complex, the "effective" concentration of thiolate may in fact be approximately 100-fold lower than the corresponding total GSH concentrations used to calculate steady-state kinetic parameters. Accordingly, the turnover numbers calculated on the basis of E·GS^- concentrations at equilibrium are underestimated by 100-fold. The k_{cat}/K_m^{GSH} second-order rate constants would then be closer to diffusion-limited values.

The overall mechanism for thiolate anion formation of GSH complexed to hGSTM1a-1a and other His107-containing chimeric GSTs may include many features. For instance, a proton exchange with His107 acting as a general base would involve the transfer of the proton through a water molecule in a relatively hydrophobic domain (see Figure 6). Accordingly, certain as yet undefined molecular realignments may be required for proper orientation of the groups involved in the proton transfer that could influence the proton dissociation. Although thiolate anion formation has been the focus of many studies of GST catalysis, the withdrawal of a proton from GSH followed by the formation of thiolate can provide only a fraction of the change in activation energy required for GST-catalyzed reactions. A recent high-resolution structure indicated that the sulfur atom of GSH is protonated when bound to a human class Pi GST, and it was proposed that a network of residues and bound water rather than a single residue functions as the proton acceptor (*52*). Those authors suggested that deprotonation occurs during formation of the ternary complex with the second substrate (*52*). In the case of hGSTM1a-1a, however, thiolate formation occurs in the absence of the second substrate, but depends on the presence of His107. In general, if GST catalysis was mainly a thiolate-dependent reaction, the expected second-order rate constants would be much lower than those observed with most substrates; thus, other events likely to occur during catalysis, notably lowering the $\Delta G'$ of the transition state, could also involve the His107 residue. A protonated imidazole of His107 could also interact with the σ-complex intermediate with the delocalized negative charge on the ring of the Meisenheimer salt intermediate.

In contrast to the nucleophilic aromatic displacement reactions, the His107Ser replacement has much less of an impact on catalysis of the ethacrynic acid (EA)−GSH addition reaction. Thus, the formation of thiolate may not be as important for this type of enzyme-catalyzed nucleophilic addition reaction (Tables 1 and 3) despite the strong pH dependence of the nonenzymatic rate constants for EA (Table 3). The K_m^S value for EA is much lower than those for the substrates that undergo aromatic substitution reactions (Table 1), but the turnover numbers are also very low even though EA is a much more reactive compound in the nonenzymatic Michael addition reaction (Table 3). In this case, rates of product release, or orientation of substrates in the catalytic cleft for reaction, could be rate-limiting (*53*).

It appears that pertinent features of the catalytic mechanism of GSTs depend on the particular isoenzyme involved, the nature of the substrate, and the type of reaction catalyzed. This point is underscored by the pivotal catalytic functions of the His107 residue that are unique for the hGSTM1a-1a enzyme.

ACKNOWLEDGMENT

We thank Drs. Steven Almo and Alexander Federov for collecting and scaling the X-ray diffraction data and Dr. Michael Toney for use of the stopped-flow spectrophotometer and assistance with the transient kinetics. We are also grateful to Drs. Vern Schramm and Sam Seifter for their comments and thorough review of the manuscript.

REFERENCES

1. Mannervik, B., and Danielson, V. H. (1988) *Crit. Rev. Biochem. 23*, 283−337.
2. Armstrong, R. N. (1994) *Adv. Enzmol. Relat. Areas Mol. Biol. 69*, 1−44.
3. Hayes, J. D., and Pulford, D. (1995) *Crit. Rev. Biochem. Mol. Biol. 30*, 445−600.
4. Jakoby, W. B., and Ziegler, D. M. (1990) *J. Biol. Chem. 265*, 20715−20718.
5. Rushmore, T. H., and Pickett, C. B. (1993) *J. Biol. Chem. 268*, 11475−11478.
6. Listowsky, I. (1993) in *Hepatic Anion Transport and Bile Secretion: Physiology and Pathophysiology* (Tavolini, N. N., and Berk, P. D., Eds.) pp 397−405, Raven Press, New York.
7. Ketterer, B., and Christodoulides, L. G. (1994) *Adv. Pharmacol. 27*, 37−69.
8. Prestera, T., and Talalay, P. (1995) *Proc. Natl. Acad. Sci. U.S.A. 92*, 8965−8969.

9. Board, P., Coggan, M., Johnston, P., Ross, V., Suzuki, T., and Webb, G. (1990) *Pharmacol. Ther. 48*, 357−369.
10. Daniel, V. (1993) *Crit. Rev. Biochem. Mol. Biol. 28*, 173−207.
11. Mannervik, B., Alin, P., Guthenberg, C., Jensson, H., Tahir, M. R., Warholm, M., and Jornvall, H. (1985) *Proc. Natl. Acad. Sci. U.S.A. 82*, 7202−7206.
12. Mannervik, B., Awasthi, Y. C., Board, P. G., Hayes, J. D., Di Ilio, C., Ketterer, B., Listowsky, I., Morgenstern, R., Muramatsu, M., Pearson, W. R., Pickett, C. B., Sato, K., Widersten, M., and Wolf, C. R. (1992) *Biochem. J. 282*, 305−306.
13. Pearson, W. R., Vorachek, W. R., Xu, S.-J., Berger, R., Hart, I., Vannis, D., and Patterson, D. (1993) *Am. J. Hum. Genet. 53*, 220−233.
14. Tu, C.-P. D., and Reddy, C. C. (1985) *J. Biol. Chem. 260*, 9961−9964.
15. Xu, S., Wang, Y. P., Roe, B., and Pearson, W. R. (1998) *J. Biol. Chem. 273*, 3517−3527.
16. Rowe, J. D., Nieves, E., and Listowsky, I. (1997) *Biochem. J. 325*, 481−486.
17. Warholm, M., Guthenberg, C., and Mannervik, B. (1983) *Biochemistry 22*, 3610−3617.
18. Raha, A., and Tew, K. D. (1996) *Cancer Treat. Res. 87*, 83−122.
19. Graminski, G. F., Kubo, Y., and Armstrong, R. N. (1989) *Biochemistry 28*, 3562−3568.
20. Armstrong, R. N. (1997) *Chem. Res. Toxicol. 10*, 2−18.
21. Bjornested, R., Tardioli, S., and Mannervik, B. (1995) *J. Biol. Chem. 270*, 29705−29709.
22. Wang, R. W., Newton, D. J., Pickett, C. B., and Lu, A. Y. (1991) *Arch. Biochem. Biophys. 286*, 574−578.
23. Zhang, P., Graminski, G. F., and Armstrong, R. N. (1991) *J. Biol. Chem. 29*, 19475−19479.
24. Kong, K. H., Inoue, H., and Takahashi, K. (1991) *Biochem. Biophys. Res. Commun. 181*, 748−755.
25. Liu, S., Zhang, P., Ji, X., Johnson, W. W., Gilliland, G. L., and Armstrong, R. N. (1992) *J. Biol. Chem. 267*, 4296−4299.
26. Kolm, R. H., Sroga, G. E., and Mannervik, B. (1992) *Biochem. J. 285*, 537−540.
27. Caccuri, A. M., LoBello, M., Nuccetelli, M., Nicotra, M., Rossi, P., Antonini, G., Frederici, G., and Ricci, G. (1998) *Biochemistry 37*, 3028−3034.
28. Comstock, K. E., Widersten, M., Hao, X. Y., Henner, W. D., and Mannervik, B. (1994) *Arch. Biochem. Biophys. 311*, 487−495.
29. Takahashi, Y., Campbell, E. A., Hirata, Y., Takayama, T., and Listowsky, I. (1993) *J. Biol. Chem. 268*, 8893−8898.
30. Patskovska, L., Federov, A. A., Patskovsky, Y. V., Almo, S. C., and Listowsky, I. (1998) *Acta Crystallogr. D54*, 458−460.
31. Rowe, J. D., Patskovsky, Y., Patskovska, L. N., Novikova, E., and Listowsky, I. (1998) *J. Biol. Chem. 273*, 9593−9601.
32. Jensson, H., Alin, P., and Mannervik, B. (1985) *Methods Enzymol. 113*, 504−507.
33. Habig, W. H., Pabst, M. J., and Jakoby, W. B. (1974) *J. Biol. Chem. 249*, 7130−7139.
34. Chen, W. J., Graminski, G. F., and Armstrong, R. N. (1988) *Biochemistry 27*, 647−654.
35. Cleland, W. W. (1970) in *The Enzymes* (Boyer, P. D., Ed.) 3rd ed., Vol. II, pp 52−54, Academic Press, New York and London.
36. Lakowicz, J. R. (1983) *Principles of Fluorescence Spectroscopy*, Plenum Press, New York.
37. Kabsch, W. (1988) *J. Appl. Crystallogr. 21*, 916−924.
38. Matthews, B. W. (1968) *J. Mol. Biol. 33*, 491−492.
39. Brunger, A. T. (1992) *XPLOR: version 3.1. A system for X-ray crystallography and NMR*, Yale University Press, New Haven, CT.
40. Engh, R. A., and Huber, R. (1991) *Acta Crystallogr. A47*, 392−400.
41. Cambillau, C., and Horjales, E. (1987) *J. Mol. Graphics 5*, 174−177.
42. Penington, C. J., and Rule, G. S. (1992) *Biochemistry 31*, 2912−2920.
43. Dirr, H., Reinemer, P., and Huber, R. (1994) *Eur. J. Biochem. 220*, 645−661.
44. Wilce, M. C. J., and Parker, M. W. (1994) *Biochim. Biophys. Acta 1205*, 1−18.
45. Parsons, J. F., Xiao, G., Gilliland, G. L., and Armstrong, R. N. (1998) *Biochemistry 37*, 6286−6294.
46. Raghunathan, S., Chandross, J., Kretsinger, R. H., Alliston, T. J., Penington, C. J., and Rule, G. S. (1994) *J. Mol. Biol. 238*, 815−832.
47. Storer, A. C., and Ménard, R. (1994) *Methods Enzymol. 244*, 486−500.
48. Sinning, I., Kleywegt, G. J., Cowan, S. W., Reinemer, P., Dirr, H. W., Huber, R., Gilliland, G. L., Armstrong, R. N., Ji, X. J., Board, P. G., Olin, B., Mannervik, B., and Jones, A. (1993) *J. Mol. Biol. 232*, 192−212.
49. Mishida, M., Harada, S., Noguchi, S., Satow, Y., Inoue, H., and Takahashi, K. (1998) *J. Mol. Biol. 281*, 135−147.
50. Rossjohn, J., Polekhina, G., Feil, S. C., Allocati, N., Masulli, M., Dillio, C., and Parker, M. W. (1998) *Structure 6*, 721−734.
51. Xiao, G., Liu, S., Ji, X., Johnson, W. W., Chen, J., Parsons, J. F., Stevens, W. J., Gilliland, G. L., and Armstrong, R. N. (1996) *Biochemistry 35*, 4753−4765.
52. Prade, L., Huber, R., Manoharan, T. H., Fahl, W. E., and Reuter, W. (1997) *Structure 5*, 1287−1295.
53. Widersten, M., Kolm, R. H., Bjornstead, R., and Mannervik, B. (1992) *Biochem. J. 285*, 377−381.

BI982164M